SolarPACES 2023, 29th International Conference on Concentrating Solar Power, Thermal, and Chemical Energy Systems

Thermal Energy Storage Materials, Media, and Systems

https://doi.org/10.52825/solarpaces.v2i.917

Published: 24 Jul. 2024

Development and Investigation of Nitrate Phase Change Filler Material for Solar Process Heating Applications

N. Pradeep[1] and K. S. Reddy[1]

[1]Indian Institute of Technology Madras

Abstract. Thermocline thermal energy storage system is an imperial system for solar process heating applications. The thermal energy storage system comprises filler material and heat transfer fluid. In the present study, the commercial phase change material (PCM) (filler material) solar salt (60%$NaNO_3$+40%KNO_3) is synthesized, and it is encapsulated with a 1mm thickness of stainless steel 316L encapsulation with the macro-size of 60mm; the encapsulated PCMs is considered as a single particle in the thermocline thermal energy storage system. The performance of the single encapsulated PCM is studied with a constant heat transfer fluid (Therminol-VP1) flow rate of 0.00015 kg/s during the charging process. The specific heat of the solar salt is measured in Differential Scanning Calorimeter (DSC) in the solid phase is found as 1.381 J/gK, and liquid phase is identified as 1.551 J/g-K, the enthalpy during the phase change process is found as 116.72 J/g. As well, the thermal conductivity of the solar salt is measured in Transient Heat Conduction method, and the thermal conductivity follows the linear relationship of -0.0025(T)+0.4023 ($45^oC<T<100^oC$) in the sensible region. The temperature variations and the phase change phenomena for the solar salt are identified, and the contours are provided. The charging time for the encapsulated solar salt is identified as ~138 minutes. The energy storage cost for the single filler material (Solar Salt + SS316L encapsulation) is identified as Rs.5.93/- (USD 0.071) for the period of charging duration.

Keywords: Solar Thermal Energy, Thermocline Thermal Energy Storage System, Phase Change Phenomena, Solar Salt, Process Heating Applications

1. Introduction

In renewable energy, solar thermal energy fluctuates seasonally, daily, and hourly wise, which are unable to meet the current energy demand (i.e., required energy for the process) consistently [1]. The thermal energy storage device successfully addressed the solution for intermittence issue, and enhances the efficiency of the process heating applications. Thermal energy storage allows for the flexibility and dispatchability of CSP systems, making them viable options for delivering clean and sustainable energy. Thermocline thermal energy storage system integrated process heating plant comprises solar concentrator, energy storage system, pumps, and process heating units [2], [3]. The thermocline thermal energy storage system consists of filler material and heat transfer fluid. The filler materials are arranged in an energy storage tank in a random/fashion manner. During the charging process, the hot fluid transfers the energy to the filler material, and the vice versa for the discharging process. In our previous study, the novel algorithm developed for the Low/Medium/High temperature filler material selection, and the results are validated with our lab experiments [4]. During experiments, the stability of the energy storage is more essential to improve the storage quality, and it is

measured with the term of thermocline. The new non-dimensional parameters are derived to measure the storage quality in X and Y direction, as well as the diagonal plane [5]. Moreover, the detailed phenomenal study in the filler material is essential to improve the storage efficiency via maintaining the thermocline quality, and increase the charging/discharging characteristics of the energy storage system.

In view of that, several researchers have been conducted both experimental and computational study for low-temperature PCMs such as, Zygmunt Lipnicki et al, [6] conducted the experimental study, to identify the solidification of phase change material (Material: RT64HC, Tm=64^{o}C) inside the capsule, where, Tm is the melting point of the phase change material. The result of the solidification front is observed in experimental, and it is compared with numerical solution. The experimental study has been carried out for RT27 (Tm=27^{o}C) with the shell size of 30mm and 70mm, and covered the various melting trend for the PCM [7]. The numerical study is conducted for the spherical bulb filled paraffin wax (T_m=62^{o}C - 64^{o}C) with darcy law porous medium model, and found that the conduction in spherical bulb dominates convection. The phase change boundary driven is strengthen by convection due to the development of melting process, the numerical solution is validated with visualize the experimental results [8]. The computational domains are developed with either unconstrained melting and constrained melting model, and experiments are conducted with static heating process.

In the present work, the solar salt is developed in our laboratory, and the characterization studies are conducted to measure the specific heat (C_p) and thermal conductivity (k). Further, the stainless steel encapsulation is developed for solar salt. The filled encapsulation is placed in the energy storage device. In the device, the heat transfer fluid flows from the top to bottom of the tank, and the temperature variations in the encapsulated solar salt is found. The experimental results are validated with the developed computational domain in ANSYS- Fluent 21. The computational domain is used to visualize the phase change phenomena (Solid Liquid) during charging process.

2. Description of Thermocline Thermal Energy Storage Device

In concentrated solar power, the solar concentrator concentrates the sunrays on to the receiver, where heat transfer fluid is heated. Due to the erratic nature of the solar irradiation, the energy output from the solar thermal energy system is unstable. The mismatch between the energy demand and supply is overcome by a thermocline thermal energy storage device, which increases the reliability of the process. The energy storage device comprises an energy storage tank, filler material, and heat transfer fluid as shown in Fig.1. The solar salt is used as a filler material and it is encapsulated with stainless steel SS316L material with the diameter of 60mm and thickness of 1mm. The encapsulated solar salt is arranged in a random/fashion manner as shown in Fig.2. The heated heat transfer fluid transfers the energy to the heat exchanger, and the energy is transferred to the power/process heating units [3]. During the day time, the heat transfer fluid flows from/to the top/bottom of the energy storage tank, and the energy is stored in the filler material in the form of internal energy (i.e., Charging process). During the process, the filler materials gain the energy [5]. Whenever intermittence occurs, and at night, the heat transfer fluid flows from/to the bottom/top of the tank (i.e., discharging process). The gained energy transfers to the process heating unit and continuously makes the process heating process successful.

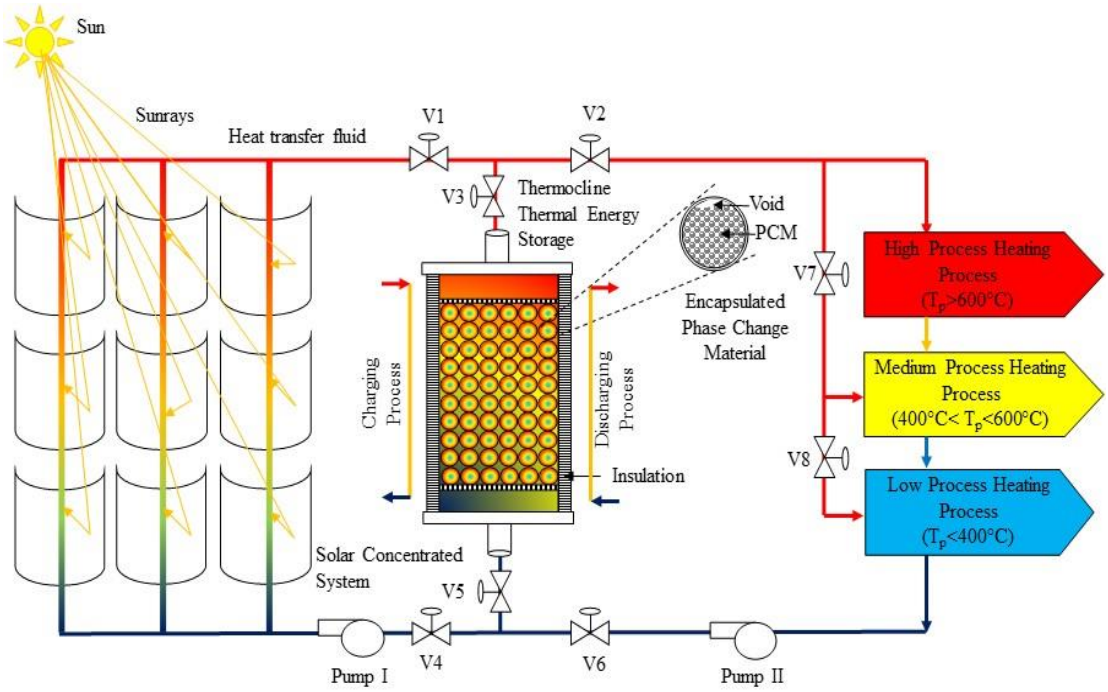

***Figure 1**. Schematic layout of solar process heating system with encapsulated solar salt-based thermocline thermal energy storage device*

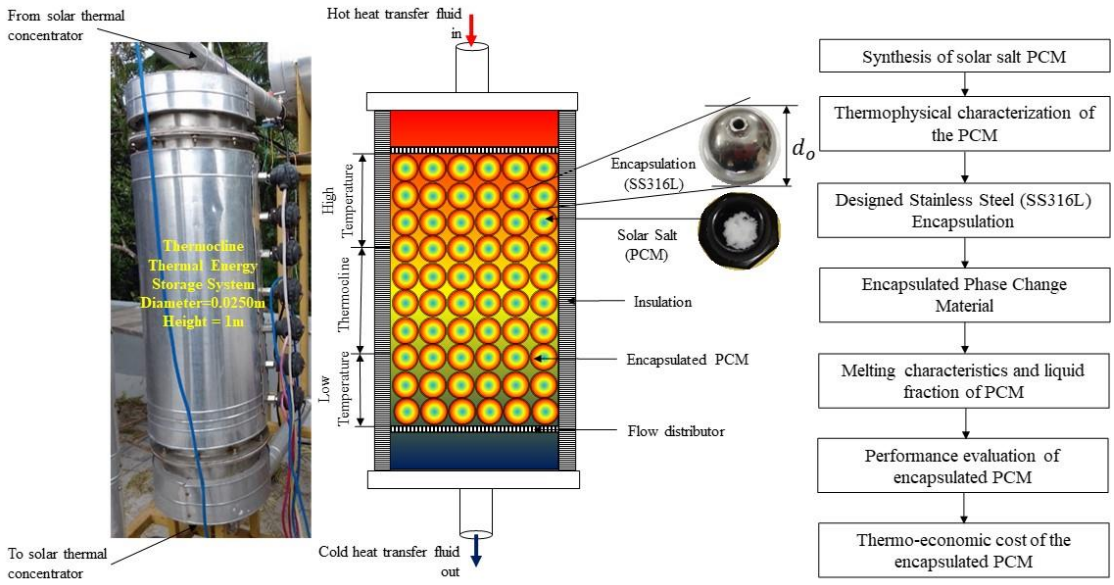

***Figure 2**. Thermocline thermal energy storage device (Location: Heat Transfer Thermal Power Laboratory, IIT Madras, Chennai (12.9915° N, 80.2337° E)), and the flowchart for the study*

3. Preparation and Characterization of Solar Salt

The ≥ 99% purity of $NaNO_3$ and ≥ 98% purity of KNO_3 were purchased from Merck Life Science Private Limited. The purchased $NaNO_3$ and KNO_3 with the correct proportions of 60% and 40% are mixed thoroughly and melted in a furnace until the temperature of 300ºC. The melted PCM is stored in the container in a controlled environment, and it is processed for the characterization study.

The specific heat of the solar salt is carefully measured in Differential Scanning Calorimeter (DSC) (Model No/company: DSC204 F1/NETZSCH) in air atmosphere with a

heating rate of 10°C/minute. The system has been calibrated properly with the atmospheric reference temperature of 20°C, and the prepared samples are measured. During the heating process (charging process), the specific heat of the solid phase is increased until the temperature of phase change 212°C (Melting temperature), and the specific heat is reduced in the liquid phase while increasing the temperature after the phase change process is completed. The average specific heat in the solid region is identified as 1.381 J/gK, and the liquid region is identified as 1.551 J/g-K. The specific heat variation with temperature is provided in Fig. 3 (a), the first peak (Peak A) in the trend shows that the volatile substance of moisture content is evaporated, and the second transition peak (Peak B) is corresponding to the solid-solid (α-KNO_3 changed to β-KNO_3) phase change, and the third peak (Peak C) shows the corresponding phase change solid-liquid (solidus temperature to liquids temperature). Finally, the measured value of the latent heat during the phase change of solar salt is identified as 116.72 J/g. However, the values are closer to various researcher's experimental study [9], which shows the methods of preparation and characterization are conducted in an appropriate way, and the prepared salt is used for the experimental analysis.

Thermal conductivity of the prepared solar salt is measured in C-Therm TCi analyzer [10]. The analyzer is functioned with MTPS technique with the spiral heater arrangement and it is supported by the guard ring. The heater provides heat to the sample, and also acts as a sensor, which detects the change in voltage, and measures the temperature of the sample. The temperature variation in the direction of heat flow (Y-direction) is measured, and the corresponding thermal conductivity values are provided by the instrument. In a manner, the thermal conductivity of the sample is measured in a sensible region due to the operational temperature limit of the instrument [11]. The thermal conductivity of the solar salt is identified as 0.240 W/mK at 30°C, and is reduced to 0.170 W/mK at 100°C. The thermal conductivity decrement in the solar salt is formulated as a linear equation, and it is K_s=-0.0025(T)+0.4023 (45°C<T<100°C), and the corresponding R^2 is 0.9487.

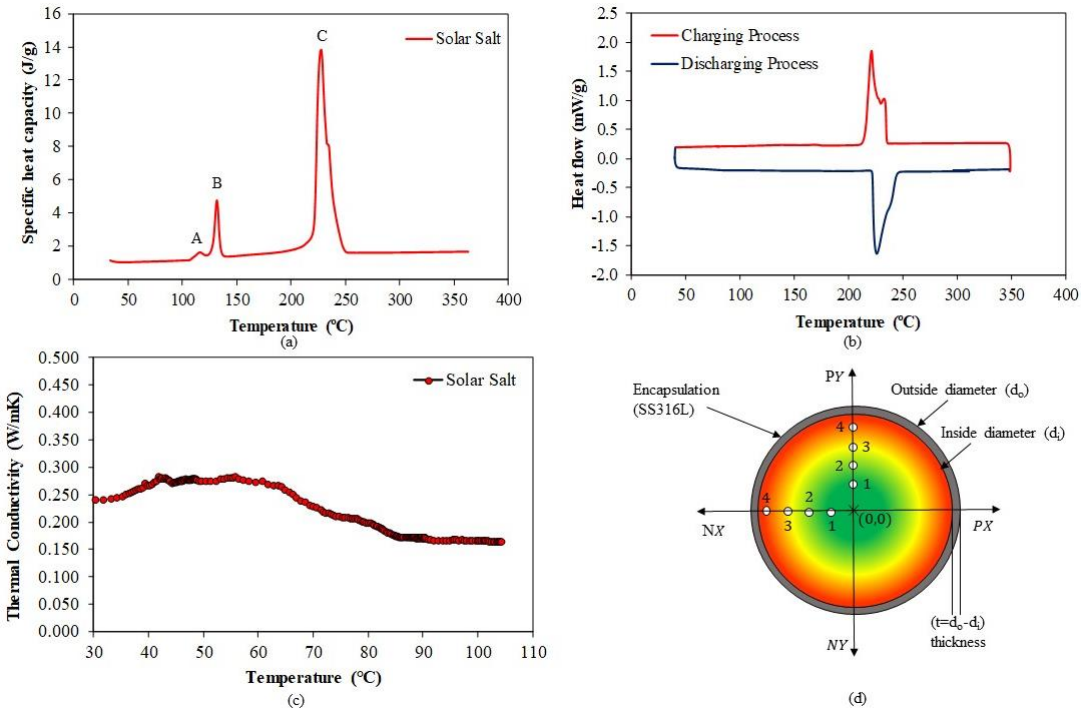

***Figure 3**. (a) Specific heat of solar salt with temperature, (b) Heat flow in solar salt for both heating (Charging process) and cooling (Discharging process), (c) Thermal Conductivity of solar salt in sensible region (d) Arrangement of thermcouple inside the spherical geometry in X and Y direction.*

4. Experimental Analysis of the designed encapsulated solar salt

The developed thermal energy storage tank of diameter 0.250m and height 1m (H/D ratio of the thermal energy storage tank is 4) is used in the experimental study (Location: IIT Madras, Chennai (12.9915° N, 80.2337° E)). As mentioned, the encapsulated solar salt is arranged in the random manner, and the 250^{o}C heated hot transfer fluid (Therminol VP1) is entering into the tank with the flowrate of 0.00015kg/s during charging process. During this process, the arranged encapsulated solar salt absorbs energy, and the temperature of the PCM is raised. In the study, eight thermocouples are fixed inside the encapsulation, Four thermocouples are fixed in X-direction, and another four thermocouples are placed in Y-direction, as shown in Fig.3 (d), which are used to measure the temperature of the solar salt during charging and discharging process.

The temperature history with respect to time is recorded in a data logger, and it is shown in Figs.4 and 5. The outermost thermocouple in both X and Y direction (NX4 and PY4) is responded quickly due to the way of energy transfer from the heat transfer fluid to the solar salt. The hot heat transfer fluid interacts with the encapsulation surface area of 0.0113 m^2 through the heat transfer mode of conduction and convection. The conducted heat is transferred to the solar salt, which reaches the fourth thermocouple (located near to the encapsulation surface) as much as possible due to the conduction mode of heat transfer. The reached energy in the 4th thermocouple location is transferred to the remaining solar salt towards the center of the encapsulation. The energy transfers to raise the temperature of the solar salt from initial temperature (T_{atm}) to phase change temperature (~212^{o}C±5^{o}C) is sensible heat transfer. The time factor (τ) is proposed to easily understand the charging time during the charging process.

$$\tau = \frac{Time\ at\ Particular\ Instant}{Time\ to\ reach\ the\ liquidus\ temp\ from\ initial\ temp} \quad (1)$$

The sensible heat transfer takes place in the solid (T_{intial}=32^{o}C) to solid phase (($T_{solidphase}$<212^{o}C±5^{o}C)) for the time of 1702 seconds (τ=0-0.20). Afterward, the phase change occurs till 4283 second (τ=0.51). Finally, after 5160 seconds (τ=0.62), the solar salt reaches completely liquid temperature, which is measured with the NX4 thermocouple. Subsequently, the temperatures are measured in the corresponding locations with the appropriate thermocouples. The entire solar salt is converted into the liquid phase, which was confirmed with thermocouple temperature. At 7783 seconds(τ=0.93), the entire solar salt in X direction is converted into liquid phase, which has been confirmed from thermocouples with NX1, NX2, NX3, and NX4 thermocouples same temperature as shown in Fig.4. Likewise, in Y direction take 8282 seconds (τ=1), as shown in Fig.5. So, the total time for the charging process is 8282 seconds.

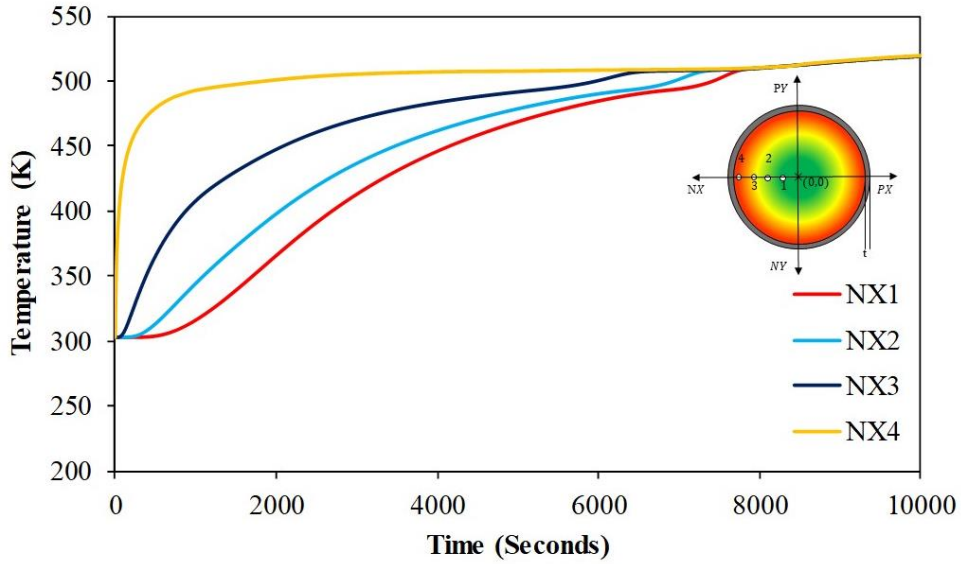

***Figure 4**. Experimental temperature variation of SS316L encapsulated solar salt in X direction*

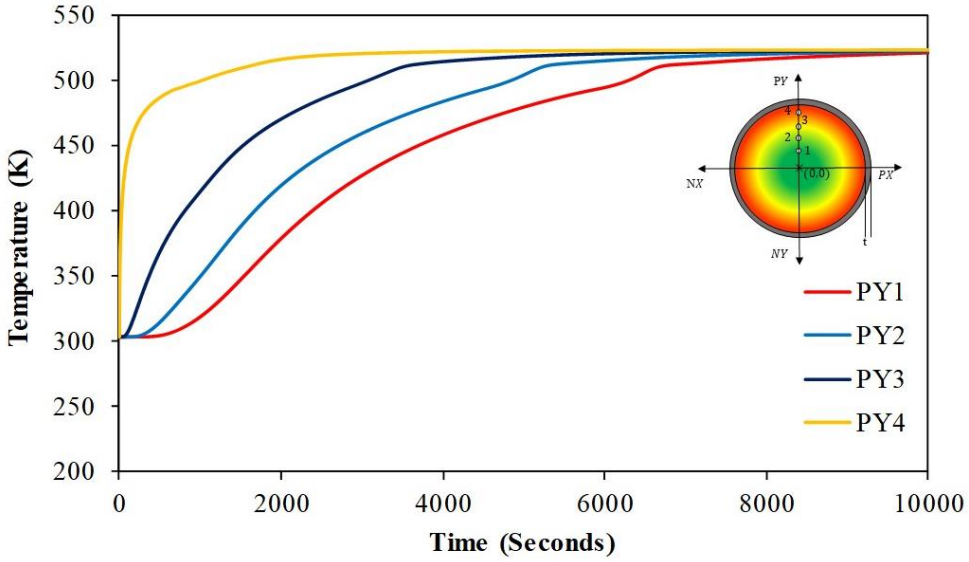

***Figure 5**. Experimental temperature variation of SS316L encapsulated solar salt in Y direction*

5. Methodology and Results of Computational domain

The experimental conditions are simulated in Ansys-21 computational domain, and it is validated to understand the phase change phenomena of the solar salt in a SS316L spherical encapsulation. The computational domain is used to predict the melting along with the phase movement in the PCM, which helps to further increase the effectiveness of the encapsulated PCM. A SS316L spherical encapsulation diameter and thickness of 0.060m and the of 0.0010m is developed, and it is analyzed with the heat transfer fluid flowrate of 0.00015 kg/s in gravity of 9.81 m/s^2 as similar to the experimental conditions. The model adopted phase change, moving phase boundary (volume of fluid is adopted), mobility of the solid phase, and heat transfer in both solid and liquid phase i.e., conduction and convection process, and it is mentioned in Fig.6.

The phase fraction in the volume for the final cell is considered as β_n, the values of β_n is considered as 0 (solid) and 1 (liquid). The intermittent value for the cell represents the mixture of two phases (solid and liquid). The enthalpy-porosity techniques are used to capture

the phases based on the porosity i.e., 0 (solid phase) and 1 (liquid phase). The fundamental governing equations Eqs.2-6 for the model is:

Continuity Equation

$$\frac{\partial \beta_n}{\partial t} + u_i \frac{\partial \beta_n}{\partial x_i} = 0 \quad (2)$$

Momentum Equation

$$\frac{\partial}{\partial t}(\rho u_i) + \frac{\partial}{\partial x_j}(\rho u_j u_i) = \mu \frac{\partial^2 u_i}{\partial x_j \partial x_j} - \frac{\partial p}{\partial x_i} + \rho g + S_i \quad (3)$$

Energy Equation

$$\frac{\partial}{\partial t}(\rho H) + \frac{\partial}{\partial x_j}(\rho u_i H) = \frac{\partial}{\partial x_i}\left(k \frac{\partial T}{\partial x_i}\right) \quad (4)$$

Where, the enthalpy term 'H' is $\hbar_{ref} + \int_{T_{ref}}^{T} C_p \, dT$, and the corresponding energy change is γL.

The phase change condition 'φ' is

$$\varphi = \{\gamma = 0 \ if \quad T < T_s \ \gamma = \frac{T - T_s}{T_l - T_s} \quad if \ \ \gamma = 1 \ if \ T > T_l \ T_s < T < T_l \quad (5)$$

and, the source term 'S_i' is $-A_\gamma u_i$, here A_γ- porosity function and converted momentum equation applicable for porous domain [12].

$$A_\gamma = \frac{C(1-\gamma)^2}{\gamma^3 + \varepsilon} \quad (6)$$

Where, $\varepsilon = 0.001$ is used as a constant in the computational domain to avoid zero and nonconvergence in Eq.5, C is considered >10^5 is used to play in the melting process.

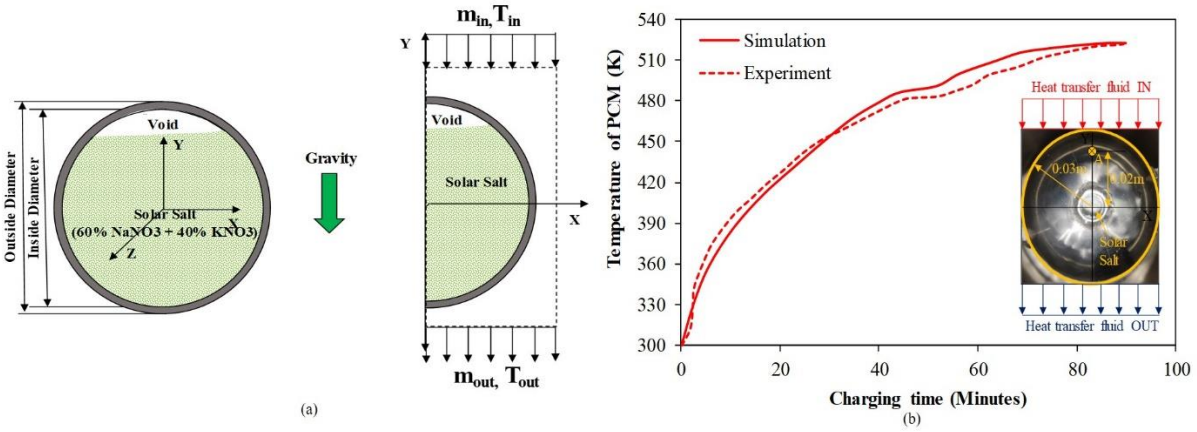

***Figure 6**. (a) Computational domain for Phase change process analysis, (b) Developed computational domain is validated with experimental work carried out in our lab*

The developed computation domain is validated well with experimental work, and it is shown in Fig.6. The domain is solved with various step sizes, and found 0.002 is best for the particular size domain. The solution convergence was checked, and convergence criteria for the problem is 10^{-5} and 10^{-8} for velocity and energy components. During the charging process, the 250°C temperature of heat transfer fluid flows perpendicular to the X-axis, and static

temperature variation and liquid fraction is identified from initial to the final time, as shown in Fig.7. The solid phase exhibits a higher rate of temperature propagation compared to the liquid phase. The sensations are characterized by a liquid layer, which envelops the molten solar salt in the upper part inside the encapsulation,while the existing solid material steadily melts and migrates towards the lower part inside the encapsulation towards the boundary. With increasing temperature and time, the melting front expands, and the liquid state of the solar salt is increased. The movement of the solid phase is distinguished by swirling patterns generated by the temperature difference between the encapsulation and liquid phase PCM, as well as the movement of the neighboring liquid PCM. At 8282 seconds (τ=1.0), the entire solar salt is converted into a liquid phase, and the phase of solar salt is liquid, which matches well with experiments.

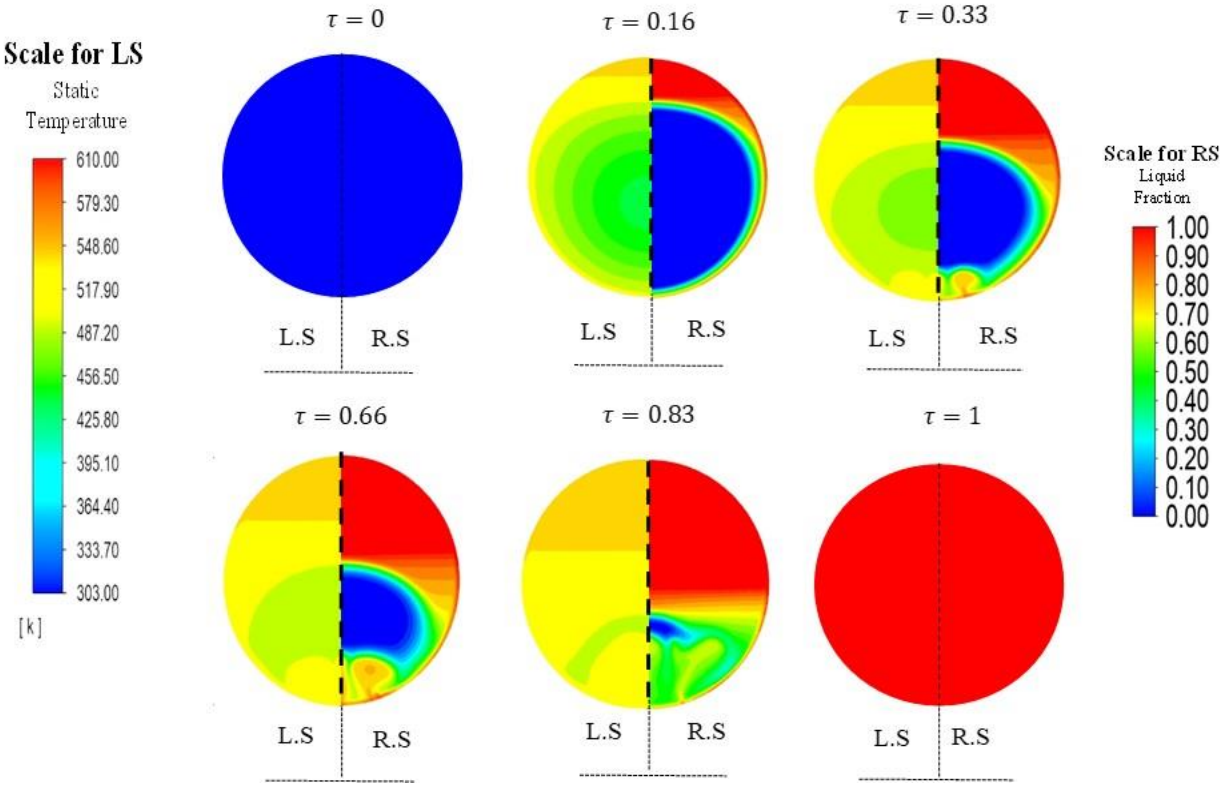

***Figure 7**. Temperature and Liquid fraction of the SS316L encapsulated solar salt phase change material*

The cost of the single encapsulated solar salt is calculated with respect to the cost of solar salt Rs.45/kg, and encapsulation material cost of Rs.250/kg. The mass of the solar salt required for the defined size (d_o=0.060m, and d_i=0.059m) is 0.193 kg, and the encapsulation material is 0.044 kg. The total weight identified for the single encapsulated solar salt is 0.238 kg. The energy stored by the solar salt is identified based on Eq.(7).

$$Energy\ Stored\ in\ Single\ Encapsulated\ Solar\ Salt = \left[m_{pcm}\left(C_{ps-pcm}(T_{intial} - T_{solid-end}) + LH_{pcm} + C_{pl-pcm}\left(T_{liquid} - T_{liquid-final}\right)\right)\right] + \left[m_{ss}(C_{ps-ss}(T_{intial} - T_{solid-end})\right] \quad (7)$$

The energy stored in the single encapsulated solar salt is found as 104.60 kJ for the entire charging process. The cost of the encapsulated solar salt is also found as Rs.5.93 for the period of charging process.

6. Conclusions

The experiment has been conducted, and the computational domain is validated well. The important findings are found from the present work as follows

- The adequate charging time for the 60mm diameter and thickness of 1mm stainless steel encapsulated solar salt is ~138 minutes (at a heat transfer fluid flow rate of 0.00015kg/s). In an identical condition, the discharging time is less than the charging time due to the inherent property of the phase change material and encapsulation material.

- The initial and atmospheric temperature of the PCM affects the charging and discharging characteristics of the energy storage system.

- The rate of energy transfer in the liquid phase is higher than in the solid phase due to the specific heat and thermal conductivity of the phases. (Solid Phase: C_{ps}= 1.381 kJ/kg, k_s= 0.24 W/mK and Liquid Phase: C_{pl}=1.551 kJ/kg, k_l=0.48 W/mK)

- The energy storage cost for the single filler material (Solar Salt + SS316L encapsulation) is identified as Rs.5.93/- (USD 0.071) for the period of charging duration.

Data availability statement

Data sharing is not applicable

Underlying and related material

No underlying or related material available

Author contributions

N. Pradeep: Conceptualization, Methodology, Modelling, Validation, Data curation, Writing – original draft.

K.S. Reddy: Conceptualization, Methodology, Visualization, Supervision, Writing – review & editing.

Competing interests

The authors declare that they have no competing interests.

References

[1] K. S. Reddy, V. Jawahar, S. Sivakumar, and T. K. Mallick, “Performance investigation of single-tank thermocline storage systems for CSP plants,” Sol. Energy, vol. 144, pp. 740–749, 2017, doi: https://doi.org/10.1016/j.solener.2017.02.012.

[2] N. Pradeep and K. S. Reddy, “Performance enhancement of packed bed thermal energy storage system for solar cogeneration of power and potable water production,” J. Clean. Prod., vol. 404, p. 136754, 2023, doi: https://doi.org/10.1016/j.jclepro.2023.136754.

[3] N. Pradeep and K. S. Reddy, “Design and investigation of solar cogeneration system

with packed bed thermal energy storage for ceramic industry," Renew. Energy, vol. 192, pp. 243–263, 2022, doi: https://doi.org/10.1016/j.renene.2022.04.087.

[4] N. Pradeep and K. S. Reddy, "Development of an effective algorithm for selection of PCM based filler material for thermocline thermal energy storage system," Sol. Energy, vol. 236, pp. 666–686, 2022, doi: https://doi.org/10.1016/j.solener.2022.02.044.

[5] K. S. Reddy and N. Pradeep, "Stability analysis of the thermocline thermal energy storage system during high flow rates for solar process heating applications," Sol. Energy, vol. 226, pp. 40–53, 2021, doi: https://doi.org/10.1016/j.solener.2021.08.026.

[6] Z. Lipnicki, T. Małolepszy, M. Gortych, and P. Grabas, "Simple analitycal and experimental method of solidification PCM material inside a spherical capsule," Int. Commun. Heat Mass Transf., vol. 135, p. 106083, 2022, doi: https://doi.org/10.1016/j.icheatmasstransfer.2022.106083.

[7] E. Assis, G. Ziskind, and R. Letan, "Numerical and Experimental Study of Solidification in a Spherical Shell," J. Heat Transfer, vol. 131, no. 2, p. 24502, 2008, doi: 10.1115/1.2993543.

[8] J. M. Khodadadi and Y. Zhang, "Effects of buoyancy-driven convection on melting within spherical containers," Int. J. Heat Mass Transf., vol. 44, pp. 1605–1618, 2001.

[9] B. D'Aguanno, M. Karthik, A. N. Grace, and A. Floris, "Thermostatic properties of nitrate molten salts and their solar and eutectic mixtures," Sci. Rep., vol. 8, no. 1, p. 10485, 2018, doi: 10.1038/s41598-018-28641-1.

[10] C-Therm Technologies Ltd, C-THERM TRIDENT, C-Therm (2022) 1–5. https://ctherm.com/thermal-conductivity-instruments/trident/.

[11] S. Jayachandran and K. S. Reddy, "Estimation of Out-of-Plane Effective Thermal Conductivity of Wire Mesh Using 3D Unit-Cell Model Incorporating Secondary Effects," J. Therm. Sci. Eng. Appl., vol. 15, no. 4, p. 41008, 2023, doi: 10.1115/1.4056773.

[12] A. D. Brent, V. R. Voller, and K. J. Reid, "ENTHALPY-POROSITY TECHNIQUE FOR MODELING CONVECTION-DIFFUSION PHASE CHANGE: APPLICATION TO THE MELTING OF A PURE METAL," Numer. Heat Transf., vol. 13, no. 3, pp. 297–318, 1988, doi: 10.1080/10407788808913615.